Available online at www.sciencedirect.com

SciVerse ScienceDirect

Ceramics International 39 (2013) 5343–5357

CERAMICS INTERNATIONAL

www.elsevier.com/locate/ceramint

Effect of niobium valence on the mechanochemical activation of niobium oxides–hematite magnetic ceramic nanoparticles

Agnieszka Grabias[a,b], Tianhong Xu[a,c], Monica Sorescu[a,*]

[a]Duquesne University, Department of Physics, 600 Forbes Avenue, 309 B Fisher Hall, Pittsburgh, PA 15282, USA
[b]Institute of Electronic Materials Technology, Wólczynska 133, 01-919 Warsaw, Poland
[c]FlexEl, LLC, 387 Technology Drive, College Park, MD 20742, USA

Received 9 November 2012; received in revised form 10 December 2012; accepted 11 December 2012
Available online 22 December 2012

Abstract

Three types of nanostructured systems: $x\mathrm{NbO}\cdot(1-x)\alpha\text{-}\mathrm{Fe_2O_3}$, $x\mathrm{NbO_2}\cdot(1-x)\alpha\text{-}\mathrm{Fe_2O_3}$, and $x\mathrm{Nb_2O_5}\cdot(1-x)\alpha\text{-}\mathrm{Fe_2O_3}$ were synthesized by ball milling at different molar concentrations ($x=0.1$, 0.3, 0.5, and 0.7). The effect of Nb valence and milling time on mechanochemical activation of these systems were studied by X-ray diffraction and the Mössbauer spectroscopy measurements. In general, Nb-substituted hematite was obtained at lower molar concentrations for all Nb oxides. For the NbO–$\mathrm{Fe_2O_3}$ system the favorable substitution of Fe^{2+} for Nb^{2+} in the octahedral sites in the NbO lattice was observed after 12 h milling for $x=0.7$. In the case of the $\mathrm{NbO_2}$–$\mathrm{Fe_2O_3}$ and $\mathrm{Nb_2O_5}$–$\mathrm{Fe_2O_3}$ systems a formation of orthorhombic $\mathrm{FeNbO_4}$ compound was observed, in which Fe^{3+} cations were detected. For the highest concentration of $\mathrm{NbO_2}$ ($x=0.7$) iron was completely incorporated into the $\mathrm{FeNbO_4}$ phase after 12 h milling. The molar concentrations of $x=0.3$ and 0.5 were the most favorable for the formation of ternary $\mathrm{FeNbO_4}$ compound in the $\mathrm{Nb_2O_5}$–$\mathrm{Fe_2O_3}$ system. Influence of ball milling on thermal behavior of the powders was investigated by simultaneous DSC–TG measurements up to 800 °C.
© 2012 Elsevier Ltd and Techna Group S.r.l. All rights reserved.

Keywords: A. Milling; B. Spectroscopy; C. Magnetic properties; D. Niobates

1. Introduction

Iron oxide nanoparticles have found recently new fields of application as compounds in catalysts or gas sensing materials [1–4]. The catalytic and photoelectrochemical properties of hematite, $\alpha\text{-}\mathrm{Fe_2O_3}$, are linked to its n-type semiconductor behavior. In recent years the attention has been focused on development of doped hematite [2,4–6] and other ternary and quarternary complex oxides [7–11] that may be used in gas sensor, catalysts and photodetector technologies. Niobium is one of the potential elements that can be used as a dopant or an additive to modify hematite [2,12–14]. It was shown that by means of a co-precipitation method Nb can be gradually introduced in the hematite structure to form $\mathrm{Fe_{2-x}Nb_xO_3}$ oxides [12]. Isomorphic substitution of Fe^{3+} ions by Nb^{5+} was related to a significant increase of catalytic activity and selectivity of the ternary oxide, which was found to be an active and selective catalyst for dehydration of isopropanol to propene [12]. Homogeneous single crystals of Nb-substituted hematite were obtained by chemical vapor transport from the ternary solution of $\mathrm{Fe_{2-x}Nb_xO_3}$ for $x<0.02$ [13]. It was reported that Nb^{5+} substitution in the octahedral sites in the corundum $\alpha\text{-}\mathrm{Fe_2O_3}$ structure led to a partial reduction of Fe^{3+} to Fe^{2+} without spinel phase inclusions [13]. The effect of the Nb/(Fe+Nb) ratio on photoelectrochemical properties of $\mathrm{Fe_2O_3}$–$\mathrm{Nb_2O_5}$ coating films has been studied in [14]. It was reported that a formation of a nanocomposite structure consisting of $\alpha\text{-}\mathrm{Fe_2O_3}$, $\mathrm{FeNbO_4}$, and Nb^{5+}-doped hematite significantly improved photoresponse to the visible light as compared to that of single compounds [14]. Recent studies of photocatalytic properties of niobia/iron oxide composites have shown that niobium generally increases the catalytic activity and stability of iron oxide based catalysts and adds interesting

*Corresponding author. Tel.: +1 412 396 4166; fax: +1 412 396 4829.
E-mail address: sorescu@duq.edu (M. Sorescu).

0272-8842/$ - see front matter © 2012 Elsevier Ltd and Techna Group S.r.l. All rights reserved.
http://dx.doi.org/10.1016/j.ceramint.2012.12.040

features such as ionic compatibility with iron oxide structure and higher reactivity [15,16].

There are three types of niobium oxides with different structures and valence of Nb (Nb^{2+}, Nb^{4+} and Nb^{5+}): NbO, NbO_2 and Nb_2O_5. Much attention has been paid to ternary $FeNbO_4$ compound which possesses interesting electrical [17,18] and magnetic [19,20] properties as well as good sensor characteristics for H_2 and H_2S [21]. Furthermore, $FeNbO_4$ oxide exhibits three different types of crystallographic phases: monoclinic, orthorhombic and tetragonal [22]. The synthesis of this compound requires in all cases several steps of preparation, including high temperature calcination [18–23]. The formation of iron niobate due to ball milling of the starting Fe_2O_3 and Nb_2O_5 powders with the nominal composition of $FeNbO_4$ using a planetary ball milling system was reported in [24]. However, partially amorphous powders had to be annealed above 750 °C to allow the complete crystallization of orthorhombic iron niobate.

High-energy ball milling technique is a well-established method for mechanochemical synthesis of nanostructured or nanocomposite materials in which non-equilibrium phases, extended solid solutions or complex structures can be formed at fairly low temperatures. Recently, the authors have performed several studies on mechanochemical activation of various mixed oxide systems such as: $x In_2O_3 \cdot (1-x)\alpha\text{-}Fe_2O_3$ [25,26], La_2O_3–$\alpha\text{-}Fe_2O_3$ [27], $x TiO_2 \cdot (1-x)\alpha\text{-}Fe_2O_3$ [28], $x ZrO_2 \cdot (1-x)\alpha\text{-}Fe_2O_3$ [29], and $x CeO_2 \cdot (1-x)\alpha\text{-}Fe_2O_3$ [30]. In the case of the In_2O_3–$\alpha\text{-}Fe_2O_3$ system with the lowest molar concentration of In_2O_3 ($x=0.1$) In-doped hematite was formed after 12 h of high-energy ball milling [25,26]. Simultaneous substitutions between In^{3+} and Fe^{3+} into hematite and In_2O_3 lattices were reported for $0.3 \le x \le 0.7$. In the case of the $x TiO_2 \cdot (1-x)\alpha\text{-}Fe_2O_3$ system Ti-doped hematite was formed at $x \le 0.3$ whereas at $0.5 \le x \le 0.9$ also Fe substitution for Ti sites in the rutile lattice was observed [28]. Similar findings were reported for the systems containing ceria and zirconia [29,30]. On the other hand, a single perovskite phase $LaFeO_3$ was synthesized through ball milling of La_2O_3 and $\alpha\text{-}Fe_2O_3$ powders in stoichiometric ratios [27].

In the present work, three types of niobium oxides with Nb^{2+}, Nb^{4+}, and Nb^{5+} were used in order to investigate the effect of Nb valence on mechanochemical activation of the following systems: $x NbO \cdot (1-x)\alpha\text{-}Fe_2O_3$, $x NbO_2 \cdot (1-x)\alpha\text{-}Fe_2O_3$, and $x Nb_2O_5 \cdot (1-x)\alpha\text{-}Fe_2O_3$. Structural changes of the samples induced by ball milling were investigated by X-ray diffraction and the Mössbauer spectroscopy measurements as a function of milling time up to 12 h and for different molar concentrations of the starting powders ($x=0.1$, 0.3, 0.5, and 0.7). ^{57}Fe Mössbauer spectroscopy is very sensitive to local atomic environments of iron nuclei. It allows one to determine the valence of iron cations as well as the assignment of Fe sites. Therefore, it is very useful in a study of iron-containing compounds with a mixed valence of iron. Mössbauer spectroscopy was successfully applied in our previous investigations of ceramic oxide nanoparticles [26–30]. In addition to structural characterization, the thermal behavior of the niobium oxides-hematite samples was investigated by simultaneous differential scanning calorimetry and thermogravimetry (DSC-TG) measurements.

2. Experimental

Commercial powders (Alfa Aesar) of niobium oxides (purity > 99%), and hematite (99.998%) were used in order to prepare three types of nanostructured systems: $x NbO \cdot (1-x)\alpha\text{-}Fe_2O_3$, $x NbO_2 \cdot (1-x)\alpha\text{-}Fe_2O_3$, and $x Nb_2O_5 \cdot (1-x)\alpha\text{-}Fe_2O_3$. Powders of hematite and niobium oxides were milled at different molar concentrations ($x=0.1$, 0.3, 0.5, and 0.7). The SPEX 8000 mixer mill was used with a hardened steel vial with 12 stainless-steel balls (type 440). The ball-to-powder mass ratio was 5:1. The samples were collected after 2, 4, 8, and 12 h of milling.

The X-ray powder diffraction patterns of samples were obtained using a Rigaku D-2013 X-ray diffractometer with CuK_α radiation ($\lambda = 1.540598$ Å) and graphite monochromator. The scanning range was 15–70° (2θ) with a step size of 0.02°. The average grain size was estimated using the Scherrer equation. Room temperature transmission Mössbauer spectra were recorded using an MS-1200 constant acceleration spectrometer with a 10 mCi ^{57}Co source diffused in Rh matrix. Least-squares fitting of the Mössbauer spectra were performed with NORMOS 90 program. Values of hyperfine field, B_{hf}, isomer shift, IS, quadrupole shift for sextets or quadrupole splitting for doublets, QS, were determined. The IS values are given relative to the source.

Simultaneous DSC–TG experiments were performed using a Netzsch Model STA 449F3 Jupiter instrument with a Silicon carbide (SiC) furnace. Samples weighting 15 ± 1 mg were contained in a manufacturer's alumina crucible with an alumina lid. The atmosphere consisted of flowing protective argon gas at a rate of 50 ml/min. DSC and TG curves were obtained by heating samples from room temperature to 800 °C with a ramp rate of 10 °C/min. The Netzsch Proteus Thermal Analysis software was used for TG and DSC data analysis.

3. Results and discussion

3.1. $xNbO \cdot (1-x)\alpha\text{-}Fe_2O_3$ system

Ball milling of the $x NbO \cdot (1-x)\alpha\text{-}Fe_2O_3$ powders with the molar concentrations of $x=0.1$ and 0.3 leads to a partial Nb^{2+} substitution of Fe sites in the hematite lattice. All XRD patterns recorded for these samples milled for 0—12 h show two sets of diffraction peaks originating from both $\alpha\text{-}Fe_2O_3$ and NbO phases. The formation of Nb-substituted hematite is revealed by a gradual reduction of the relative intensity of NbO peaks as the milling time increases. Furthermore, the lines of both phases show progressive broadening with increasing milling time which

can be associated with a decrease of grain sizes due to high-energy ball milling. The lines related to hematite are, however, much broader than the lines of the niobium oxide for all milling times. The average grain size, $\langle D \rangle$, of the starting powders is 51 nm for hematite and >100 nm for NbO. At $x=0.1$ the grain size $\langle D \rangle$ of α-Fe_2O_3 and NbO phases decreases to 25 and 44 nm already after 2 h of milling, and then to 14 and 29 nm after 12 h, respectively. Very similar trend is observed for the samples with $x=0.3$ ($\langle D \rangle = 13$ and 23 nm after 12 h, respectively).

Fig. 1 presents XRD patterns obtained for the xNbO·$(1-x)Fe_2O_3$ samples with $x=0.5$ and 0.7 as a function of milling time. For the manually ground samples (0 h) two sets of narrow peaks originating from the starting NbO (cubic, *Pm3m*) and α-Fe_2O_3 (rhombohedral, *R3c*) powders are observed (Fig. 1(a) and (f)). Niobium oxide peaks dominate each pattern in Fig. 1. In the case of $x=0.5$ sample both phases of NbO and hematite are observed up to 12 h of milling (Fig. 1(e)). The diffraction lines become broader with increasing milling time. As it was observed for $x=0.1$ and 0.3 the lines of hematite are significantly broader than the lines of NbO, indicating that hematite grains are finer than niobium oxide ones. The average grain sizes of α-Fe_2O_3 and NbO phases decrease to 10 and 22 nm after 12 h, respectively. A decrease of the relative intensity of the NbO lines is related to incorporation of Nb^{2+} into the hematite lattice. In the case of $x=0.7$ both phases (NbO and hematite) are observed up to 8 h of milling (Fig. 1(g)–(i)). After 12 h of milling only the pattern related to NbO phase is present (Fig. 1(j))

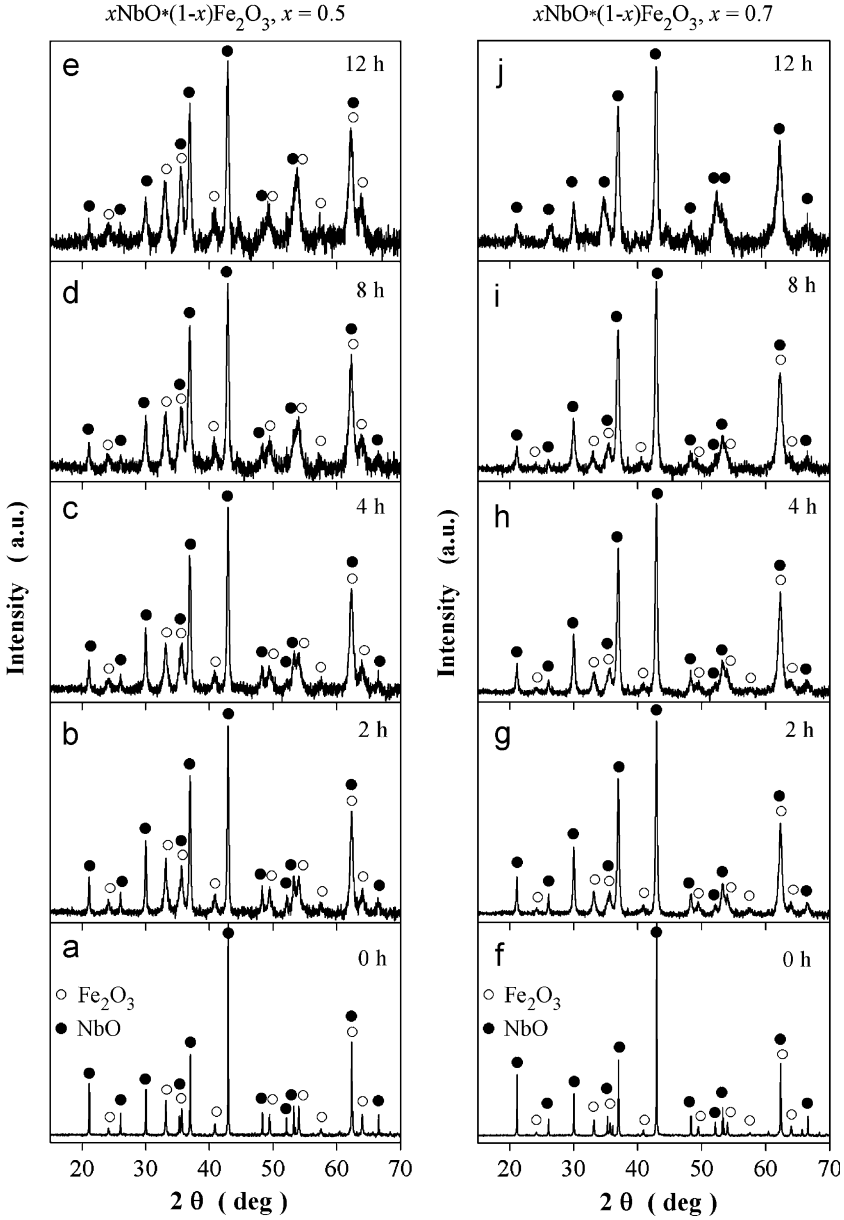

Fig. 1. XRD patterns of the xNbO·$(1-x)$α-Fe_2O_3 system for $x=0.5$ and 0.7: (a) and (f) starting mixtures; (b)–(e) and (g)–(j) after milling for 2–12 h.

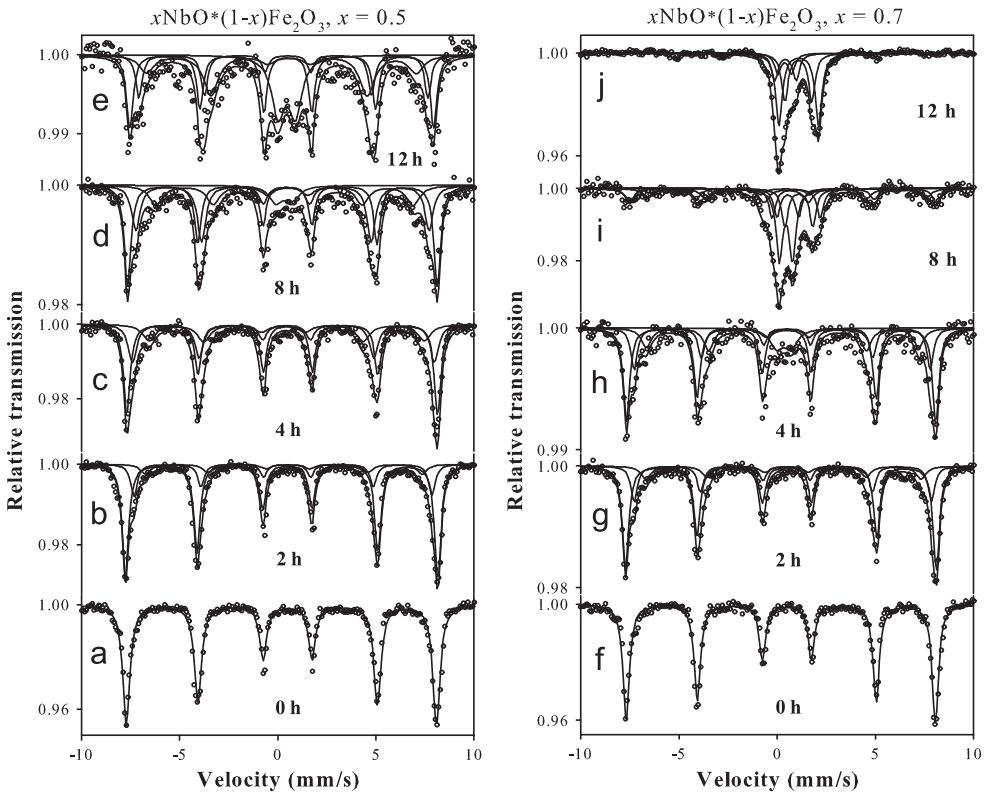

Fig. 2. Mössbauer spectra of the $x\mathrm{NbO}\cdot(1-x)\alpha\text{-}Fe_2O_3$ system for $x=0.5$ and 0.7: (a) and (f) starting mixtures; (b)–(e) and (g)–(j) after milling for 2 – 12 h.

indicating that entire iron content is incorporated into the NbO lattice. The broad lines point to a significant grain refinement of Fe-doped NbO phase. The estimated average grain size is about 20 nm (after 12 h). It should be noted that in most cases the diffraction lines related to both phases are practically not shifted. The largest shifts towards lower 2θ angles of about 0.15° for $\alpha\text{-}Fe_2O_3$ and 0.08° for NbO are observed for the samples with $x=0.5$ and 0.7 after 12 h milling. This result suggests that Nb substitution slightly expands the hematite lattice.

Fig. 2 presents examples of Mössbauer spectra of the milled $x\mathrm{NbO}\cdot(1-x)Fe_2O_3$ samples for $x=0.5$ and 0.7. Hyperfine parameters and relative abundance of each spectral component calculated for all samples are presented in supplementary Table I-S. The spectra of all manually ground starting mixtures (0 h) are fitted with one sextet with hyperfine field, B_{hf}, of about 49 T, isomer shift of 0.33–0.38 mm/s, and quadrupole shift of −0.30 mm/s, which are characteristic of nanohematite (Fig. 2(a) and (f)). A lower hyperfine field than that of conventional hematite ($B_{hf}\approx 51$ T) is usually observed for small particles due the significant fraction of Fe surface sites. In the cases of $x=0.1$ and 0.3 samples the spectral lines become broader with increasing milling time, which indicates a gradual substitution of Nb^{2+} for Fe sites in hematite. The spectra recorded after milling for 2–12 h were fitted with three sextets. A dominating sextet with B_{hf} of about 49 T is assigned to $\alpha\text{-}Fe_2O_3$. Two additional sextets with B_{hf} of about 47 and 42 – 43 T, and with similar *IS* and *QS* values as those of hematite are related to Nb-doped hematite. Nb substitution causes a decrease of the hyperfine field of hematite. The relative spectral fraction of both additional sextets increases gradually with increasing milling time and after 12 h it reaches 60% and 64% for $x=0.1$ and 0.3, respectively. The spectra obtained for these samples are very similar to the spectrum shown in Fig. 2(c), which is also fitted with the corresponding three sextets. Both Mössbauer spectra and XRD results show that a part of Nb^{2+} cations substitute hematite and Nb-doped $\alpha\text{-}Fe_2O_3$ is formed.

For $x=0.5$ the Mössbauer spectra of the samples milled for 2 and 4 h (Fig. 2(b) and (c)) were fitted with three sextets like in the case of $x=0.1$ and 0.3. The relative spectral fraction of the sextets with a reduced hyperfine field of about 47 and 41–43 T increases with milling time up to about 61% after 12 h at the expense of the pure hematite sextet. This is related to increasing substitution of Nb^{2+} for Fe sites in the hematite lattice. After 8 and 12 h of milling a new non-magnetic spectral component appears in the central part of the spectra in Fig. 2(d) and (e). The quadrupole doublet with broad lines ($\Gamma=0.8$ mm/s), quadrupole splitting of 0.94 mm/s, and IS = 0.48 mm/s is assigned to Fe^{3+} ions which are most probably located in the NbO lattice or less probably are in the isolated superparamagnetic ultrafine grains of hematite. The relative fraction of this doublet increases with milling time and

contributes about 18% to the total spectral area after 12 h of milling (Fig. 2(e)).

In the case of $x=0.7$ system ball milling causes at first the formation of Nb^{2+}-doped hematite as revealed by the appearance of two additional magnetically split sextets with reduced hyperfine fields in the Mössbauer spectra of the samples milled for 2 and 4 h (Fig. 2(g) and (h)). In distinction to the $x=0.5$ system in which the quadrupole doublet related to Fe^{3+} appeared at 8 h, in the $x=0.7$ system it is observed earlier, i.e., already after 4 h of milling (Fig. 2(h)). This minor doublet with broad lines ($\Gamma=0.8$ mm/s) is split into two doublets with narrow linewidths of 0.4 mm/s when their relative spectral contribution increases to about 39% after 8 h (Fig. 2(i)). Both doublets with $QS_1=0.67$ mm/s and $IS_1=0.45$ mm/s, and $QS_2=1.10$ mm/s and $IS_2=0.54$ mm/s can be assigned to Fe^{3+} ions which are most probably located in the NbO lattice in two atomic environments with different symmetry. On the other hand, a minor presence of isolated ultrafine grains of hematite, which are not detected by XRD method (Fig. 1(j)), exhibiting a superparamagnetic behavior cannot be unambiguously excluded. The spectrum of the sample milled for 8 h is complex and was fitted with two magnetic components and four quadrupole doublets (Fig. 2(i)). There is a certain abundance (~34%) of two magnetic components with reduced B_{hf} (48 and 44 T) that indicates a presence of Nb-doped hematite, in accordance with XRD results (Fig. 1(i)). Furthermore, besides two Fe^{3+} doublets two additional doublets with significantly larger quadrupole splitting and isomer shift values were fitted. Their relative fraction increases significantly from 27% after 8 h milling to 72% after 12 h (Fig. 2(i) and (j)). The doublets with $QS_1=2.02$ mm/s and $IS_1=1.10$ mm/s, and $QS_2=1.37$ mm/s and $IS_2=1.08$ mm/s (Fig. 2(j)) are characteristic of Fe^{2+} ions which are located in two octahedral sites in the NbO lattice. It is worth noting that the hyperfine parameters of all Fe^{3+} and Fe^{2+}doublets resemble those known from other iron-containing oxides [16,31]. As milling time increases from 8 to 12 h the increase of the relative fraction of Fe^{2+} doublets is correlated with a significant decrease of the intensities of Fe^{3+} doublets as well as with a disappearance of the magnetic components (Fig. 2(j)). The XRD measurement of the sample milled for 12 h revealed only one pattern characteristic of the NbO structure (Fig. 1(j)). Therefore, milling for 12 h caused the formation of the non-magnetic Fe-doped NbO phase.

According to Mössbauer and XRD measurements of $xNbO\cdot(1-x)Fe_2O_3$ samples for small molar concentrations of NbO ($x=0.1$ and 0.3) Nb^{2+}-doped hematite was obtained after 12 h of milling. A portion of the NbO phase remained in the powder system. When NbO concentration is large enough like in the case of $x=0.5$ both Nb^{2+}-doped hematite and Fe^{3+}-doped NbO were observed. For the highest concentration of NbO ($x=0.7$) entire iron content seems to be incorporated into the NbO lattice after 12 h milling. In addition to Fe^{3+} ions a significant spectral contribution of Fe^{2+} ions (~72%) is observed, indicating the favorable substitution of Fe^{2+} for Nb^{2+} in the octahedral sites of the NbO lattice.

3.2. $xNbO_2\cdot(1-x)\alpha$-Fe_2O_3 system

Fig. 3 presents XRD patterns obtained for the ball milled $xNbO_2\cdot(1-x)Fe_2O_3$ samples with $x=0.3$ and 0.7 as examples. The patterns of the $x=0.1$ and $x=0.5$ samples (not shown) are qualitatively similar to those of $x=0.3$ and $x=0.7$, respectively. For the manually ground samples (0 h) two sets of narrow peaks originating from the starting NbO_2 (tetragonal, rutile-like structure) and α-Fe_2O_3 powders are observed (Fig. 3(a) and (f)). Hematite peaks dominate the patterns for molar concentrations of $x=0.1$ and 0.3 while niobium dioxide peaks dominate the patterns of $x=0.5$ and 0.7. The average grain size of the starting powders is about 50 nm for hematite and >100 nm for NbO_2.

Ball milling of the powders with $x=0.1$ and 0.3 leads to a partial Nb^{4+} substitution of Fe sites in the hematite lattice. The diffraction peaks of both α-Fe_2O_3 and NbO_2 phases are seen up to 8 h of milling, however, a gradual reduction of the relative intensity of NbO_2 peaks with increasing milling time is clearly visible (Fig. 3(a)–(d)). A complete incorporation of Nb into α-Fe_2O_3 and formation of Nb-substituted hematite is observed after 12 h milling for which the XRD pattern consists only of broad hematite lines (Fig. 3(e)). Also the line intensities of Nb-doped hematite changed as compared with the original pattern of α-Fe_2O_3 (Fig. 3(a)). Progressive broadening of diffraction lines with increasing milling time points to a refinement of the grain sizes of both oxides. As in the previous case of the NbO–Fe_2O_3 system, the lines related to hematite are much broader than the NbO_2 lines, indicating that hematite grains are significantly smaller than niobium dioxide ones. A reduction of grain size $\langle D\rangle$ to 20 nm already after 2 h milling, and then to 12 nm after 12 h was observed for Nb-doped hematite for both $x=0.1$ and 0.3. For NbO_2 phase $\langle D\rangle$ of about 40 nm was estimated after milling for 2–8 h.

In the case of the powders with $x=0.5$ and 0.7 after ball milling up to 4 h a broadening of NbO_2 and α-Fe_2O_3 lines are observed (Fig. 3(g) and (h)). The grain size $\langle D\rangle$ estimated for niobium and iron oxides decreases to about 30 and 15 nm, respectively, after 4 h milling. Further ball milling (8–12 h) leads to the formation of a new phase. The number of diffraction lines characteristic to NbO_2 and Fe_2O_3 phases decreases and new broad lines appear after 8 h milling (Fig. 3(i)). The broad pattern observed after 12 h milling can be assigned to the formation of ternary $FeNbO_4$ phase with grain size $\langle D\rangle$ below 15 nm for both $x=0.5$ and 0.7 (Fig. 3(j)). Significant broadening of diffraction lines makes the determination of the crystallographic structure of the $FeNbO_4$ phase difficult. The pattern seems to fit best to the disordered orthorhombic phase (isomorphic to α-PbO_2 structure) in which Fe and

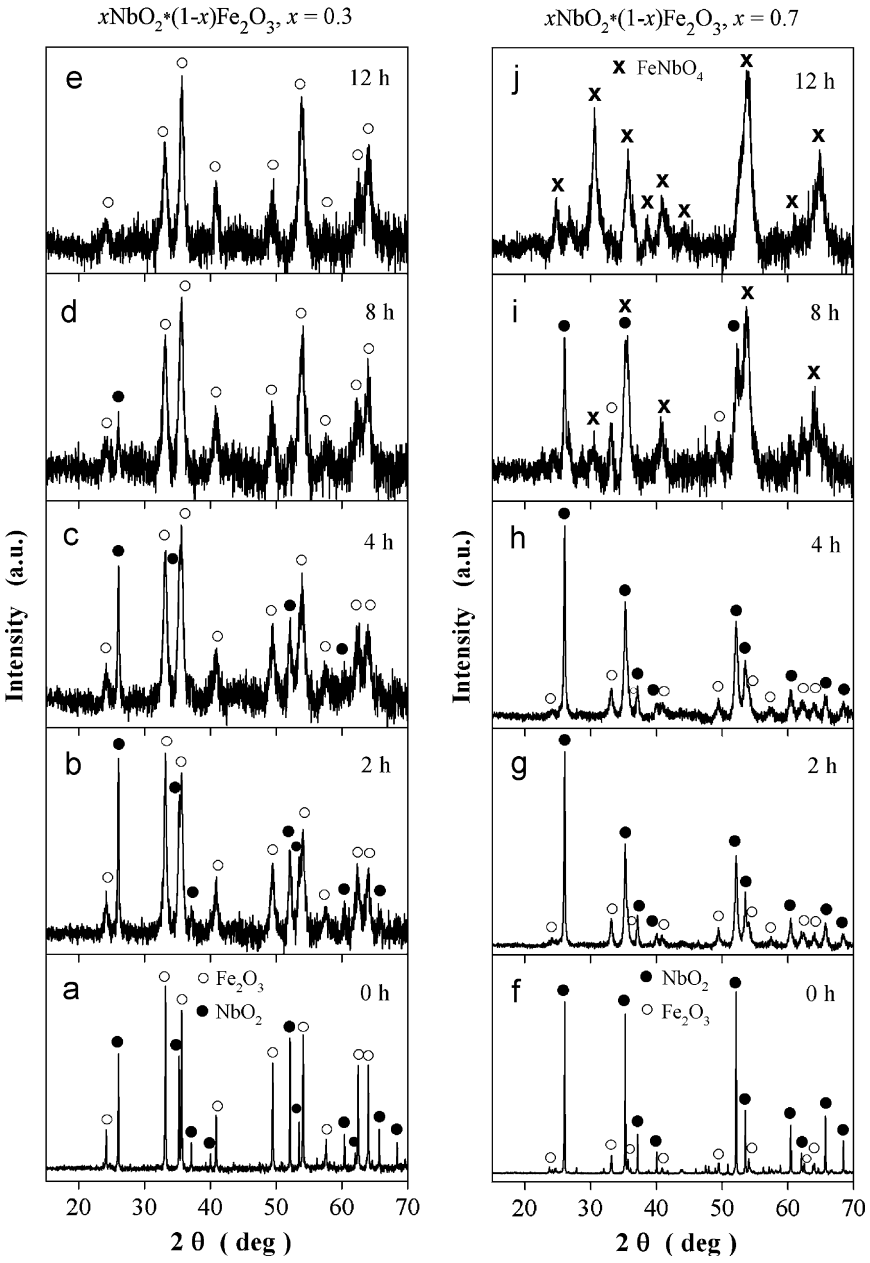

Fig. 3. XRD patterns of the $x\mathrm{NbO_2}\cdot(1-x)\alpha\text{-}\mathrm{Fe_2O_3}$ system for $x=0.3$ and 0.7: (a) and (f) starting mixtures; (b)–(e) and (g)–(j) after milling for 2 – 12 h.

Nb ions are randomly distributed in 4*c* sites. For $x=0.5$ in addition to the iron niobate phase also weak Nb-doped hematite lines are observed whereas for $x=0.7$ only $FeNbO_4$ is detected. These results indicate that higher molar concentration ($x=0.7$) favors the complete formation of ternary $FeNbO_4$ phase.

Fig. 4 presents the Mössbauer spectra of all milled $x\mathrm{NbO_2}\cdot(1-x)\mathrm{Fe_2O_3}$ samples. Hyperfine parameters and relative abundance of each spectral component calculated for all samples are presented in Table II-S. The spectra of all manually ground mixtures (0 h) are fitted with one sextet assigned to hematite (B_{hf}=49–50 T, $IS\cong 0.40$ mm/s, and $QS\cong -0.30$ mm/s). The first hours of milling result in broadening of the magnetic pattern. In the case of the lowest molar concentration of NbO_2 ($x=0.1$) the spectra were fitted with two sextets after 2 and 4 h milling (Fig. 4(b) and (c)), and with three sextets after 8 and 12 h (Fig. 4(d) and (e)). In addition to the dominating sextet with B_{hf} of about 49 T, two sextets with B_{hf} of about 46–48 and 43 T, and with similar *IS* and *QS* values as those of hematite were introduced. Appearance of these additional sextets with reduced hyperfine fields as compared with the hematite one, indicates a gradual substitution of Nb^{4+} for Fe sites in $\alpha\text{-}Fe_2O_3$. Nb substitution as a non-magnetic element causes a decrease of the hyperfine field of hematite. The relative spectral fraction of both

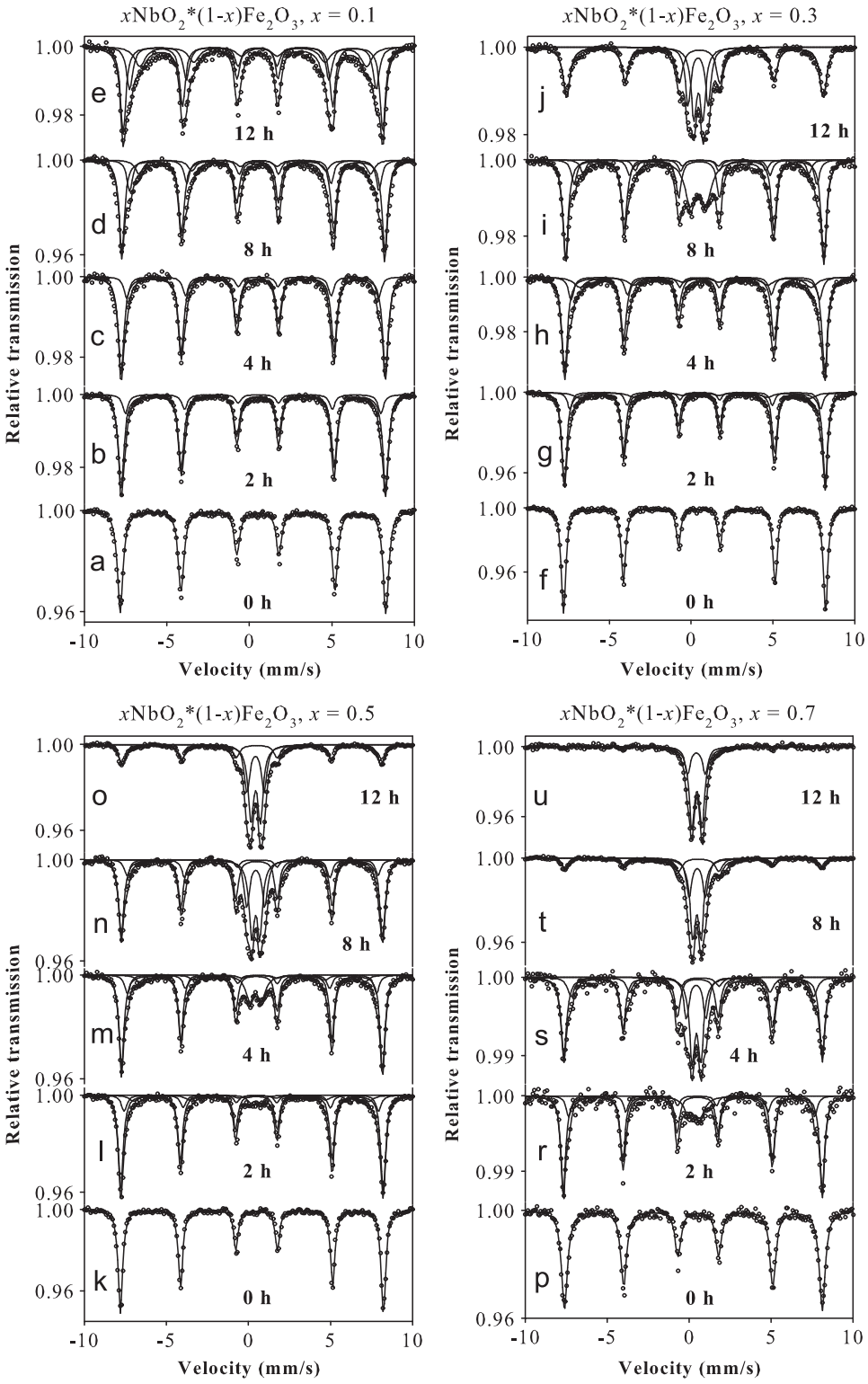

Fig. 4. Mössbauer spectra of the $x\mathrm{NbO_2}\cdot(1-x)\alpha\text{-}\mathrm{Fe_2O_3}$ system ($x=0.1$, 0.3, 0.5, and 0.7): (a), (f), (k), and (p) starting mixtures; (b)–(e), (g)–(j), (l)–(o), and (r)–(u) after milling for 2–12 h.

additional sextets increases gradually with increasing milling time at the expense of the pure hematite sextet, and after 12 h reaches 52%.

For $x=0.3$ and 0.5 the Mössbauer spectra of the samples milled for up to 4 and 8 h, respectively, were fitted with three sextets (Fig. 4(g)–(i), (l), and (m)). The relative spectral fraction of the sextets with a reduced B_{hf} of about 47 and 43 T, which are related to the formation of Nb-doped hematite, increases with milling time, however, it is much smaller than for $x=0.1$. Their largest abundance is

about 34% for $x=0.3$ after 4 h milling. The relative fraction of both sextets decreases at longer milling times due to the formation of non-magnetic components at the central part of the spectra (Fig. 4(i), (j), and (l)−(o)). The quadrupole doublet with broad lines ($\Gamma=0.8$ mm/s) appears first after 8 h for $x=0.3$ whereas for $x=0.5$ it is seen already at 2 h. This broad doublet is split into two doublets with narrow linewidths of 0.4 mm/s when the contribution of the non-magnetic component increases with increasing milling time. Both doublets with $QS_1 \cong 0.54$ mm/s and $IS_1=0.45$ mm/s, and $QS_2 \cong 1.10$ mm/s and $IS_2 \cong 0.44$ mm/s can be assigned to Fe^{3+} ions. Taking into account the XRD result for $x=0.3$ (Fig. 3(e)), which reveals only a broad pattern of Nb-doped hematite, Fe^{3+} ions may originate from ultrafine grains exhibiting superparamagnetic behavior that are located in Nb-rich environments in hematite. The second possible explanation for Fe^{3+} is that these ions are incorporated into the remained NbO_2 phase whose relative content is too small to be detected by XRD method. In the case of $x=0.5$ the Fe^{3+} ions are most probably located in the orthorhombic $FeNbO_4$ phase which was identified by XRD measurements. The disordered orthorhombic $FeNbO_4$ compound is paramagnetic down to 4.2 K [19]. In the stoichiometric $FeNbO_4$ compound Fe and Nb ions are in 3+ and 5+ valence states, respectively. Two Fe^{3+} quadrupole doublets were reported for orthorhombic $FeNbO_4$ with the α-PbO_2 structure in Ref. [18] whereas for the wolframite structure (monoclinic) only one Fe^{3+} doublet was observed at room temperature. On the other hand, for the orthorhombic columbite phase ($FeNb_2O_6$) two major Fe^{2+} doublets were reported in Ref. [31]. For all these reasons, two Fe^{3+} doublets observed for our samples in Fig. 4(n)–(o) can be convincingly assigned to Fe^{3+} ions in two different cation environments in the orthorhombic $FeNbO_4$ lattice. A small amount of a broad magnetic component observed in the Mössbauer spectrum recorded after 12 h milling (Fig. 4(o)) reveals that a portion of Nb-doped hematite is still present in the sample. The relative fraction of both Fe^{3+} doublets increases with milling time to about 45% for $x=0.3$ and about 66% for $x=0.5$ after 12 h of milling (Fig. 4(j) and (o)).

The formation of the non-magnetic ternary $FeNbO_4$ compound is much more efficient in the case of the sample with the largest NbO_2 concentration of $x=0.7$. A small broad quadrupole doublet appears already after 2 h milling (Fig. 4(r)). The relative fraction of two narrow Fe^{3+} doublets with very similar hyperfine parameters as for $x=0.7$ is about 35% after 4 h (Fig. 4(s)). It increases to 100% for the sample milled for 12 h, whose spectrum consists only of two non-magnetic components (doublets, Fig. 4(u)). Therefore, after 12 h milling the formation of the ternary $FeNbO_4$ compound is complete, in a good agreement with the XRD data (Fig. 3(j)). As concerns the magnetic spectral components, in addition to the hematite sextet a sextet with a reduced hyperfine field of about 46 T was fitted only for the samples milled for 2 and 4 h (Fig. 4(r) and (s)). This indicates partial substitution of Fe by Nb in the hematite lattice. The relative fraction of this additional sextet is, however, fairly low at about 16%, suggesting that rather limited Nb-doping of hematite occurs. The relative contribution of the magnetic spectral components decreases rapidly to about 28% after 8 h milling (Fig. 4(t)). The sextet remaining after 8 h milling is completely transformed into doublets in the spectrum recorded after 12 h (Fig. 4(u)).

Both Mössbauer spectra and XRD results show a complete formation of Nb^{4+}-doped hematite after 12 h milling of the $xNbO_2 \cdot (1-x)Fe_2O_3$ samples for $x=0.1$ and 0.3. For larger molar concentrations ($x=0.5$ and 0.7) a formation of orthorhombic $FeNbO_4$ compound is observed. For the highest concentration of NbO_2 ($x=0.7$) iron is completely incorporated into the $FeNbO_4$ phase after 12 h milling.

3.3. $xNb_2O_5 \cdot (1-x)$α-Fe_2O_3 system

Fig. 5 presents XRD patterns obtained for the $xNb_2O_5 \cdot (1-x)Fe_2O_3$ samples after 12 h milling. An example of the pattern of manually ground samples (0 h) is shown in Fig. 5(a) which consists of two sets of narrow peaks originating from the starting Nb_2O_5 (orthorhombic, *Pbam*) and α-Fe_2O_3 powders. The average grain size of the starting powders is about 50 nm for hematite and 72 nm for Nb_2O_5. Ball milling of the powder with $x=0.1$ leads to Nb substitution of Fe sites in the hematite lattice (Fig. 5(b)). Intensities of diffraction peaks of Nb_2O_5 decrease gradually with increasing milling time up to about 8 h. A complete incorporation of Nb^{5+} into α-Fe_2O_3 and formation of Nb-substituted hematite is observed after 12 h milling for which the XRD pattern consists only of broadened hematite lines (Fig. 5(b)). Relative intensities of Nb-doped hematite lines changed as it was observed for the NbO_2–Fe_2O_3 system (Fig. 3(e)). A reduction of the grain size $\langle D \rangle$ to 20 nm already after 2 h milling, and then to 12 nm after 12 h is observed for Nb-doped hematite.

For $x=0.3$ and 0.5 the XRD patterns obtained after 12 h milling are qualitatively similar (Fig. 5(c) and (d)). Like in the case of $x=0.1$, intensities of diffraction peaks of Nb_2O_5 decrease gradually with increasing milling time up to about 8 h, and the grain size $\langle D \rangle$ decreases to about 16 nm. However, after 8 h milling new broad lines appear in the patterns, whose positions are the same as those observed for $xNbO_2 \cdot (1-x)Fe_2O_3$ at a larger molar concentration of Nb dioxide ($x=0.5$ and 0.7, Fig. 3(j)). After 12 h milling two phases can be identified: Nb-doped hematite and $FeNbO_4$-like phase with orthorhombic structure (Fig. 5(c) and (d)). The grain size $\langle D \rangle$ estimated for $FeNbO_4$ phase is about 10 nm. For Nb-doped hematite it is 10 and 18 nm at $x=0.3$ and 0.5, respectively.

In the case of the powders with $x=0.7$ a mixture of Nb_2O_5 and hematite phases is observed for all milling times (Fig. 5(e)). Progressive line broadening as milling time increases yields the grain size $\langle D \rangle$ of about 15 and

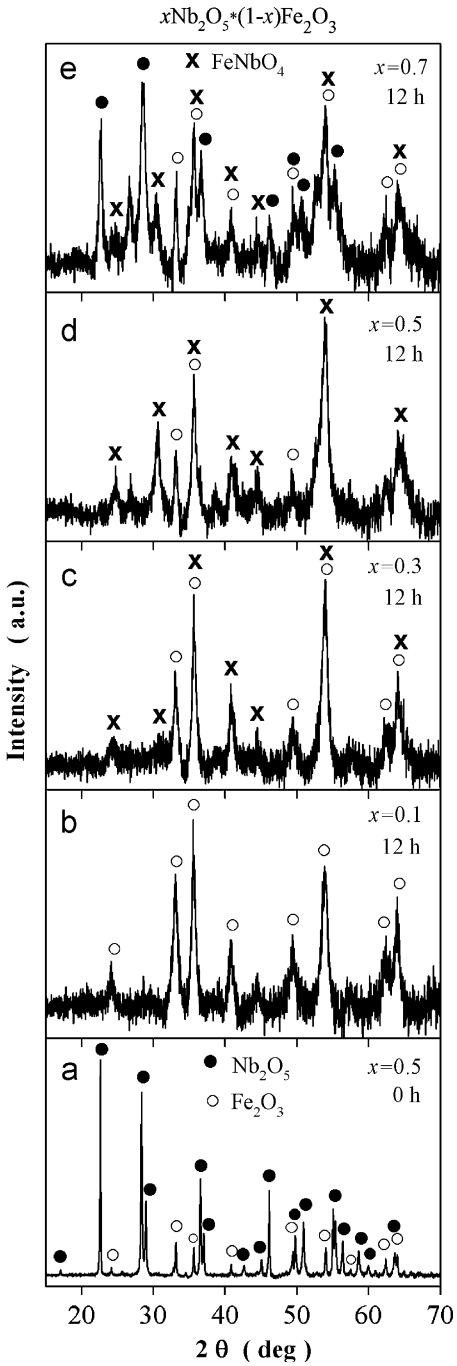

Fig. 5. XRD patterns of the $xNb_2O_5 \cdot (1-x)\alpha$-$Fe_2O_3$ samples: (a) example of a starting mixture (0 h) with $x=0.5$; (b)–(e) powders with $x=0.1$, 0.3, 0.5, and 0.7 milled for 12 h.

20 nm for Nb_2O_5 and Nb-doped hematite, respectively, after 12 h milling. Ball milling for 12 h leads to the partial formation of $FeNbO_4$-like phase with the grain size $\langle D \rangle$ of about 10 nm, whose traces can be seen also after 8 h. One peak at 26.6° remains unidentified (Fig. 5(e)).

Examples of Mössbauer spectra of milled $xNb_2O_5 \cdot (1-x)Fe_2O_3$ powders are shown in Fig. 6 for $x=0.1$ and 0.5. Hyperfine parameters and relative abundance of each spectral component calculated for all samples are collected in Table III-S. The spectra of all manually ground mixtures (0 h) are fitted with one sextet assigned to hematite ($B_{hf} \cong 48.0$ T, $IS \cong 0.46$ mm/s, and $QS \cong -0.30$ mm/s). In the case of $x=0.1$ a broadening of the magnetic pattern with increasing milling time is observed (Fig. 6(b)–(e)). Therefore the spectra were fitted with two (2 h) or three magnetically split sextets (4–12 h). In addition to the dominating hematite sextet with B_{hf} of about 48 T, two sextets with B_{hf} of about 45 and 40 T, and with similar IS and QS values as those of hematite were introduced. The sextets with reduced hyperfine fields as compared to hematite indicate a gradual substitution of Nb^{5+} for Fe sites in α-Fe_2O_3. The relative spectral fraction of both additional sextets increases gradually with increasing milling time at the expense of the pure hematite sextet, and after 12 h reaches 42%. The case of the $xNb_2O_5 \cdot (1-x)Fe_2O_3$ system is the only one for which a quadrupole doublet is observed at the lowest molar concentration of niobium oxide ($x=0.1$). About 3% of the spectral fraction of the doublet is detected in the spectrum obtained after 8 h milling (Fig. 6(d)). After 12 h milling the broad quadrupole doublet with $QS=0.97$ mm/s and $IS=0.48$ mm/s contributes about 20% to the total spectral area (Fig. 6(e)). The hyperfine parameters are characteristic of Fe^{3+} ions. The presence of this non-magnetic component indicates that for longer milling times also Fe^{3+} substitution for Nb^{5+} sites in the Nb_2O_5 lattice occurs.

The Mössbauer spectra obtained for the samples with $x=0.3$ and 0.5 are qualitatively very similar (Fig. 6(f)–(j)). They differ slightly by relative fractions of spectral components. Relatively small abundance of additional sextets with reduced hyperfine fields (41–46 T) is observed with increasing milling time. Their relative fraction does not exceed 23%. The intensity of the main hematite sextet decreases with increasing milling time. After 12 h milling only one weak magnetically split sextet with B_{hf} of about 48 T is present in the spectra (Fig. 6(j)), revealing that a certain amount of Nb-doped hematite is contained in the samples, in a good agreement with the XRD patterns (Fig. 5(c) and (d)). The relative abundance of the sextet decreases after 12 h milling to about 24% and 26% for $x=0.3$ and 0.5, respectively. The quadrupole doublet with broadened lines ($\Gamma=0.5$ mm/s) appears first already after 2 h milling (Fig. 6(g)). This broad doublet is split into two doublets ($\Gamma=0.4$ mm/s) when the contribution of the non-magnetic component increases with increasing milling time (Fig. 6(h)–(j)). Both doublets with $QS_1 \cong 0.56$ mm/s and $IS_1=0.52$ mm/s, and $QS_2 \cong 1.10$ mm/s and $IS_2 \cong 0.52$ mm/s are assigned to Fe^{3+} ions. The relative fraction of both Fe^{3+} doublets increases significantly with milling time to about 76% for $x=0.3$ and 74% for $x=0.5$ after 12 h milling (Fig. 6(j)). Taking into account the XRD results (Fig. 5(c) and (d)), which reveal the $FeNbO_4$ pattern beside the Nb-doped hematite one, it can be concluded that Fe^{3+} ions are most probably located in two different sites in the orthorhombic $FeNbO_4$ phase. It is worth noting that quadrupole doublet appears already after 2 h milling when average grain size of α-Fe_2O_3 is about 25 nm, which is

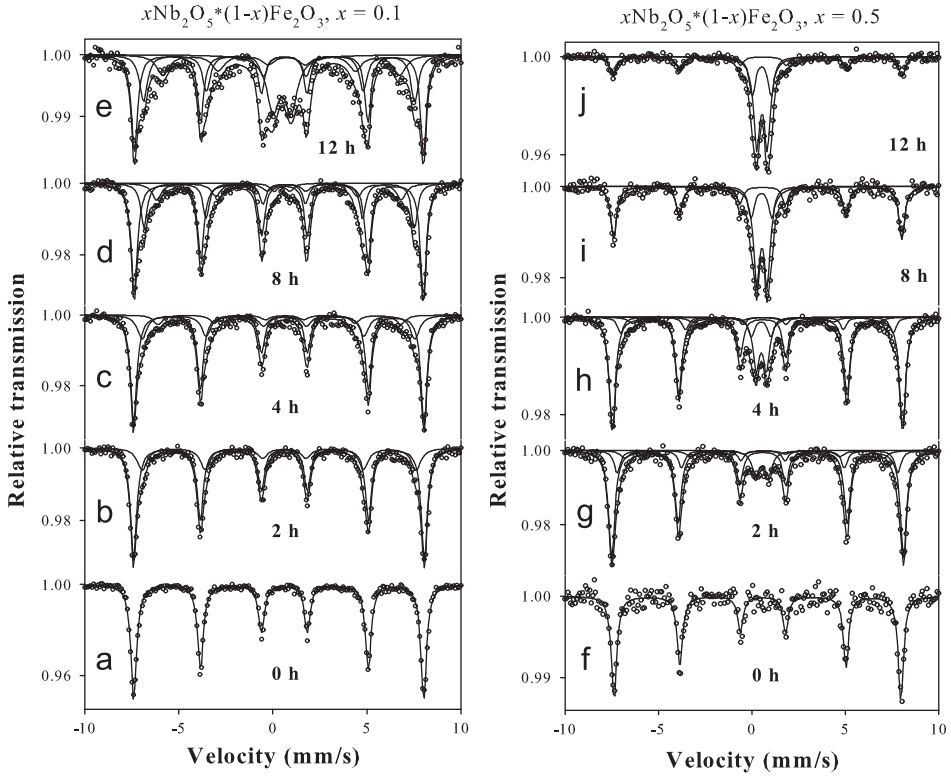

Fig. 6. Mössbauer spectra of the $x\mathrm{Nb_2O_5}\cdot(1-x)\alpha\text{-}\mathrm{Fe_2O_3}$ system for $x=0.1$, and 0.5: (a) and (f) starting mixtures; (b)–(e) and (g)–(j) after milling for 2–12 h.

rather too large to consider superparamagnetic behavior of hematite grains. Therefore, the Mössbauer results indicate simultaneous Fe^{3+} and Nb^{5+} substitutions in the niobium pentoxide and hematite lattices, respectively, as the milling process progresses.

In a clear distinction to the previous cases ($x=0.1$–0.5) for $x=0.7$ only one magnetic component related to hematite ($B_{hf}\cong 48$ T) is observed in the Mössbauer spectra of the samples milled for 2–12 h. This means that a very limited Nb-substitution of the $\alpha\text{-}\mathrm{Fe_2O_3}$ phase occurs during ball milling. The relative fraction of the hematite sextet decreases to about 51% after 12 h milling due to the formation of non-magnetic components at the central part of the spectra. The spectrum recorded after 12 h milling is very similar to that obtained for $x=0.5$ after 8 h milling (Fig. 6(i)). A broad Fe^{3+} doublet with a relative fraction of about 12% appears in the spectrum of the sample milled for 4 h. Two quadrupole doublets with $QS_1\cong 0.60$ mm/s and $IS_1=0.54$ mm/s, and $QS_2\cong 1.10$ mm/s and $IS_2\cong 0.54$ mm/s were fitted in the spectra obtained for longer milling times. Their relative fraction increases with milling time from 28% to 49% after 8 and 12 h of the milling process, respectively. These two doublets are assigned as before to Fe^{3+} cations in two different environments of iron niobate.

The XRD and Mössbauer results indicate that in the case of the $x\mathrm{Nb_2O_5}\cdot(1-x)\mathrm{Fe_2O_3}$ system the molar concentration plays a major role in the synthesis of ternary compounds. The formation of Nb-doped hematite is significantly suppressed by the constitution of non-magnetic iron niobate for $x\geq 0.3$. The results show that molar concentrations of $x=0.3$ and 0.5 are the most favorable for the formation of ternary $\mathrm{FeNbO_4}$ phase due to ball milling.

Fig. 7 compares the Mössbauer results for all studied systems of mixed niobium and iron oxides. The relative spectral fractions of Fe^{3+} or Fe^{2+} doublets are plotted vs. milling time for all molar concentrations studied. The development of non-magnetic spectral components with increasing milling time is clearly seen for all systems. The increase of the relative fractions of doublets reflects mechanically induced mixing of Nb and Fe oxides, namely the incorporation of Fe into the niobium oxides or the formation of ternary compounds. However, clear differences are observed when taking into account three types of niobium oxides with different Nb valence. For the $x\mathrm{NbO}\cdot(1-x)\alpha\text{-}\mathrm{Fe_2O_3}$ system with Nb^{2+} (Fig. 7(a)) a relatively weak contribution of Fe^{3+} doublet appears only at larger molar concentration of NbO ($x=0.5$). For $x=0.7$ a contribution of Fe^{3+} doublets is slightly higher, however, there is a major fraction of Fe^{2+} doublets. In this case entire iron content is incorporated into the NbO lattice after 12 h milling. The dominating presence of Fe^{2+} ions indicates the favorable substitution of Fe^{2+} for Nb^{2+} in the octahedral sites in the NbO lattice. The $x\mathrm{NbO}\cdot(1-x)\alpha\text{-}\mathrm{Fe_2O_3}$ system is the only one among the

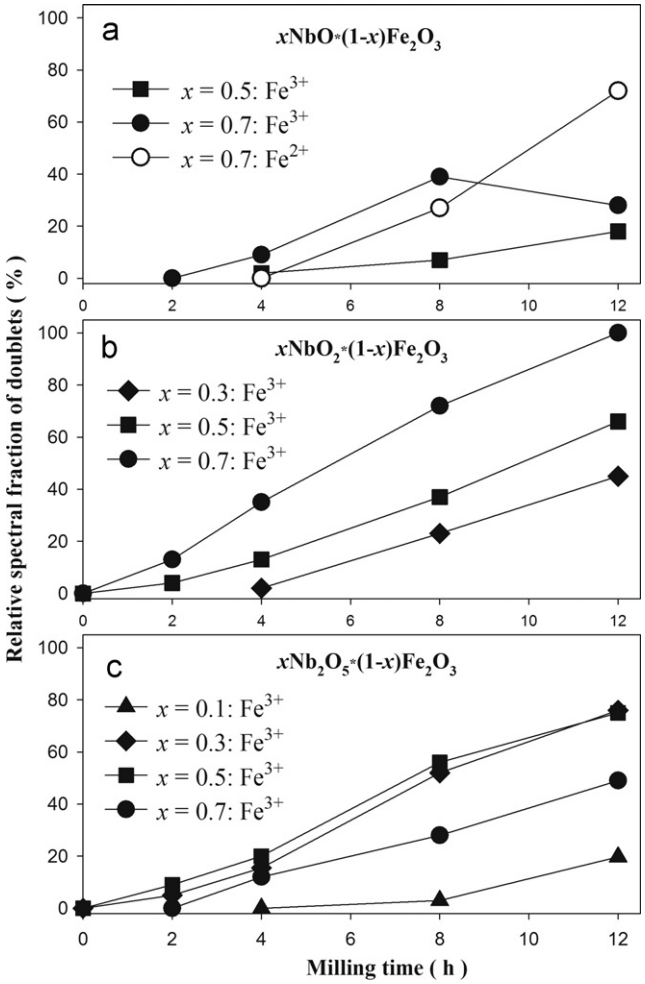

Fig. 7. Relative spectral fractions of Fe^{3+} or Fe^{2+} doublets determined from Mössbauer spectra of $NbO-Fe_2O_3$, $NbO_2-Fe_2O_3$, and $Nb_2O_5-Fe_2O_3$ powders as a function of milling time.

studied systems in which Fe^{2+} ions were detected by Mössbauer spectroscopy measurements. Plots obtained for both $x\mathrm{NbO_2}\cdot(1-x)\alpha$-$\mathrm{Fe_2O_3}$ (Fig. 7(b)) and $x\mathrm{Nb_2O_5}\cdot(1-x)\mathrm{Fe_2O_3}$ (Fig. 7(c)) systems with Nb^{4+} and Nb^{5+}, respectively, reveal similar characteristics. The relative fraction of Fe^{3+} doublets increases with increasing milling time, indicating gradual substitution of Nb by Fe^{3+} cations. In both cases the formation of ternary $FeNbO_4$ compound is observed. For the NbO_2–Fe_2O_3 system the Fe^{3+} spectral component appears for $x \geq 0.3$ whereas for the Nb_2O_5–Fe_2O_3 system it is detected already at the lowest molar concentration ($x=0.1$) and is observed for all x studied. For NbO_2–Fe_2O_3 the relative fraction of non-magnetic components increases with increasing molar concentration. A different behavior is observed for the $Nb_2O_5-Fe_2O_3$ system. The characteristics obtained for $x=0.3$ and 0.5 are almost the same. However, much lower fractions of non-magnetic components are observed for the extreme molar concentrations ($x=0.1$ and 0.7). This indicates that molar concentrations of $x=0.3$ and 0.5 are the most favorable for the formation of ternary $FeNbO_4$ non-magnetic phase due to ball milling.

3.4. Simultaneous DSC–TG measurements

Simultaneous DSC–TG measurements allowed us to study the influence of ball milling on thermal stability of the powders at temperatures ranging from room temperature to 800 °C. As examples the results obtained for $x\mathrm{NbO}\cdot(1-x)\mathrm{Fe_2O_3}$ with $x=0.1$ and $x\mathrm{Nb_2O_5}\cdot(1-x)$-$\mathrm{Fe_2O_3}$ with $x=0.5$ powders milled for 0–12 h are shown in Figs. 8 and 9, respectively. The DSC curves of the $x\mathrm{NbO}\cdot(1-x)\mathrm{Fe_2O_3}$ samples with $x=0.1$ reveal a broad exothermic peak on which a narrow exothermic peak is overlapped (Fig. 8(a)–(e)). The broad peak covers a wide range of temperatures and shifts to lower temperatures with the increase of milling time. A shift towards lower temperatures as milling time increases is observed also for the narrow peak whose maximum temperature is marked in Fig. 8. Similar DSC curves are obtained for $x=0.3$ which is consistent with the fact that these samples reveal similar structures after milling. For larger x a more complex thermal behavior is observed with three or four exothermic peaks, which requires a separate investigation in order to identify thermally induced transformations in those powders. As the broad exothermic peak is concerned, it can be related to a partial decomposition of hematite to magnetite (Fe_3O_4) as it was observed earlier [32]. It was concluded that ball-milled hematite with reduced particle sizes is more likely to decompose to magnetite. This is also the case of the ball-milled $x\mathrm{NbO}\cdot(1-x)\mathrm{Fe_2O_3}$ samples with $x=0.1$ and 0.3 for which the relevant exothermic effect starts at lower temperatures as milling time increases. The narrow exothermic peak in the range of about 500–600 °C is clearly observed not only for the samples with $x=0.1$ and 0.3 but also for the starting mixed powders (0 h) with $x=0.5$ and 0.7. Therefore it can be related to a thermally induced reaction between niobium and iron oxides. The maximum temperature of this DSC peak decreases with increasing NbO concentration from 573 °C for $x=0.1$ to 533 °C for $x=0.7$ for manually ground powders.

TG curves provide information regarding the mass change as a function of the elevated temperature (Fig. 8(f)–(j)). Pure hematite was characterized by a major weight loss step at 100–600 °C with the value of 0.93% [32]. TG curves obtained for all niobium oxides exhibited a continuous decrease up to about 600 °C without any visible step. The total weight loss for niobium oxides (0.2–0.5%) was significantly smaller than for hematite (0.93%). In the case of the manually ground mixture of $x\mathrm{NbO}\cdot(1-x)\mathrm{Fe_2O_3}$ ($x=0.1$) the TG curve reveals two weight loss steps which can be identified by the changes in the slopes of this curve (Fig. 8(f)). The first step with a weight loss value of 2.18% can be assigned to the partial decomposition of hematite to magnetite while the theoretical calculation for the complete transformation yields a larger weight loss of 3.44% [32]. The second weight loss step with a fairly small value of 0.33% is well correlated with the exothermic DSC peak in the temperature range of about 500–600 °C

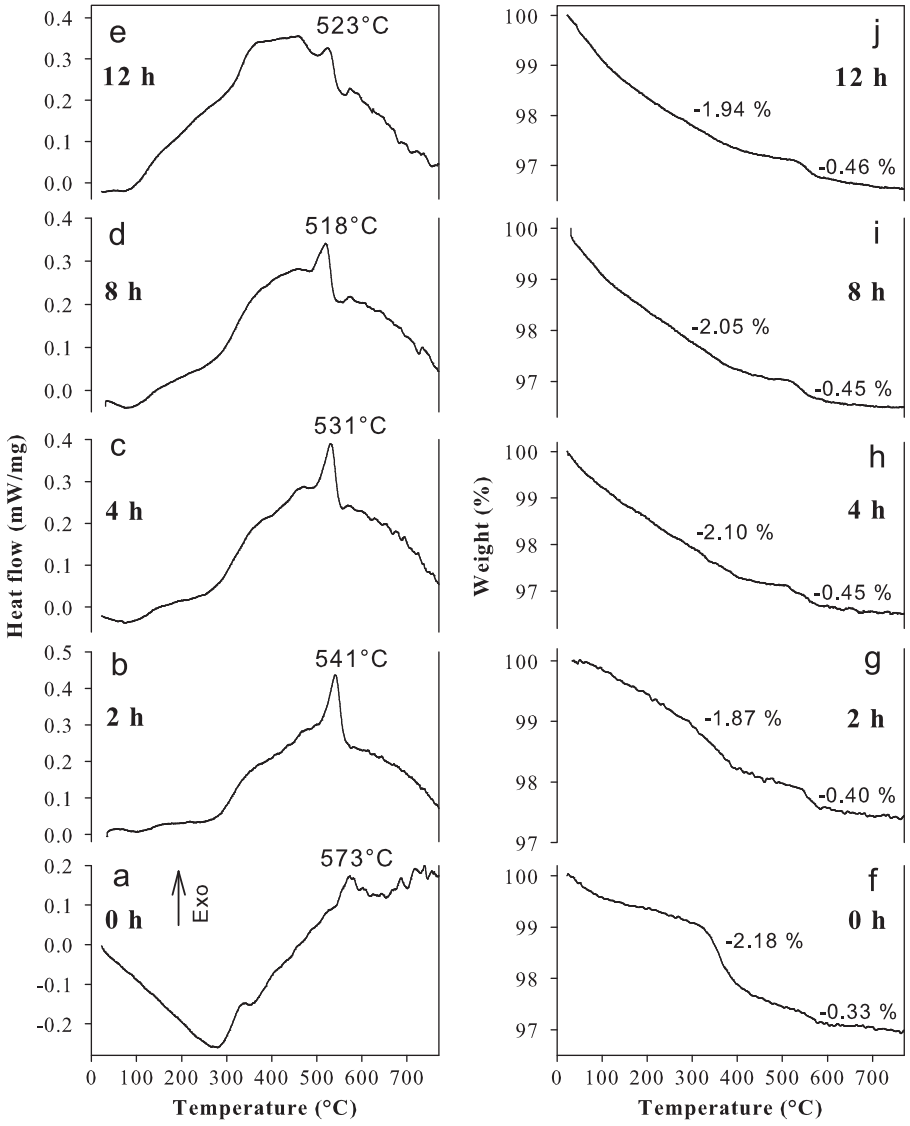

Fig. 8. DSC curves of the $x\mathrm{NbO}\cdot(1-x)\alpha\text{-}\mathrm{Fe_2O_3}$ system for $x=0.1$: (a) starting mixture (0 h); (b)–(e) after milling for 2–12 h, and the corresponding TG curves (f)–(j).

(Fig. 8(a)). As milling time increases the second weight loss step starts at lower temperatures and its value increases slightly (Fig. 8(g)–(j)). On the other hand, the first step in the TG curve in Fig. 8(f) is less visible for the sample milled for 2 h (Fig. 8(g)) and is not observed for longer milling times (Fig. 8(h)–(j)). However, the values of the weight loss in the range of about 100–400 °C calculated for the ball-milled samples are only slightly smaller than those of the starting mixed powder. These values decrease significantly with decreasing $\alpha\text{-}\mathrm{Fe_2O_3}$ concentration in the $x\mathrm{NbO}\cdot(1-x)\mathrm{Fe_2O_3}$ system (with increasing x) to 0.7–1.0% for $x=0.7$. A monotonic decrease in TG curves of the milled samples observed up to about 400 °C may indicate that the ball milling causes an extension of weight loss processes towards lower temperatures. This effect can be associated with the shift of the broad DSC peak to lower temperatures with increasing milling time. It is well known that ball milling introduces a large amount of defects in the powders and internal strain, whereas a thermal treatment induces short range ordering and heating out of vacancies. It is worth noting that the small weight loss observed up to about 100 °C is usually referred to the evaporation process of physically adsorbed water from the surface of the particles.

A different thermal behavior is observed for the $x\mathrm{Nb_2O_5}\cdot(1-x)\mathrm{Fe_2O_3}$ samples (Fig. 9). The DSC curve of the starting mixed powder for $x=0.5$ reveals a very broad exothermic peak covering almost the whole range of temperatures applied (Fig. 9(a)). Its maximum temperature (378 °C) correlates perfectly with the center of the single weight loss step in the corresponding TG curve (Fig. 9(f)). This thermal behavior characterizes a partial decomposition of hematite to magnetite and possibly also solid–solid interactions between $\alpha\text{-}\mathrm{Fe_2O_3}$ and $\mathrm{Nb_2O_5}$ particles since the calculated enthalpy of this exothermic effect (1.8 kJ/g) is larger than that obtained for pure hematite (1.2 kJ/g).[32] After ball milling

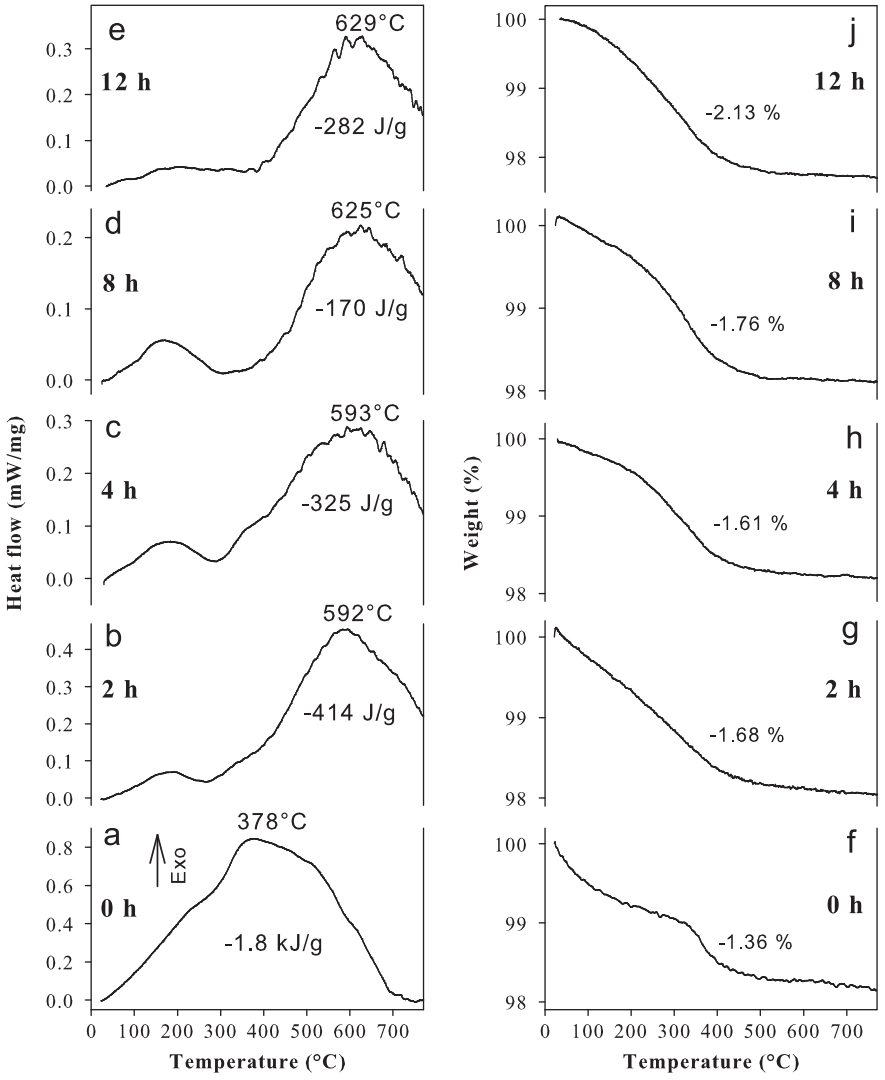

Fig. 9. DSC curves of the $x\mathrm{Nb_2O_5}\cdot(1-x)\alpha\text{-}\mathrm{Fe_2O_3}$ system for $x=0.5$: (a) starting mixture (0 h); (b)–(e) after milling for 2 – 12 h, and the corresponding TG curves (f)–(j).

for 2–12 h the DSC curves change considerably showing two exothermic effects. A weak broad peak observed up to about 300 °C originates most probably from a partial decomposition of hematite to magnetite (Fig. 9(b)–(e)). A presence of hematite in the samples milled for up to 12 h has been evidenced by XRD and Mössbauer measurements (Figs. 5 and 6). It was shown recently that a decrease of grain sizes of hematite caused a decrease of its stability upon heating under argon atmosphere [32]. In the case of our samples the average grain size of the hematite phase decreases from about 50 nm for the starting powder to 18 nm after 12 h milling. A decrease of the thermal stability due to milling is also seen in TG curves up to about 400 °C, which reveal a monotonic drop with no visible step extending towards lower temperatures as compared with the TG curve of the starting powder (Fig. 9(f)–(j)). The major broad DSC peak starting at about 400 °C shifts slightly to higher temperatures with the increase of milling time (Fig. 9(b)–(e)). The enthalpy related to this exothermic effect is dramatically smaller than that calculated for the starting mixed powder. Furthermore, the broad peak is not accompanied by a weight loss as seen in the TG curves of the milled samples for temperatures exceeding 400 °C (Fig. 9(g)–(j)). Therefore, the origin of this exothermic peak may be related to re-crystallization and grain growth processes. It is worth noting that the weight loss values decrease with the increase of x from 2.0–2.5% for $x=0.1$ to 0.5–1.2% for $x=0.7$. The highest values are observed for the samples milled for 12 h.

4. Conclusions

Three types of mixed niobium and iron oxides systems: $x\mathrm{NbO}\cdot(1-x)\alpha\text{-}\mathrm{Fe_2O_3}$, $x\mathrm{NbO_2}\cdot(1-x)\alpha\text{-}\mathrm{Fe_2O_3}$, and $x\mathrm{Nb_2O_5}\cdot(1-x)\alpha\text{-}\mathrm{Fe_2O_3}$ were synthesized by high-energy ball milling for 2–12 h at different molar concentrations ($x=0.1$, 0.3, 0.5, and 0.7). The use of three niobium oxides with different valence of Nb (Nb^{2+}, Nb^{4+}, and Nb^{5+}) allowed us to investigate the effect of Nb valence on the structure and thermal stability of the systems as a function of molar

concentrations and milling times. The samples were characterized by X-ray diffraction, Mössbauer spectroscopy, and simultaneous DSC–TG measurements. At lower molar concentrations of niobium oxides (x) Nb-substituted hematite was synthesized. At higher x non-magnetic components related to Fe^{3+} or Fe^{2+} cations were observed in the Mössbauer spectra, which were assigned to Fe ions introduced to the non-magnetic Nb oxides due to ball milling. Their relative spectral fraction increased with the increase of milling time at the expense of the magnetic components related to the hematite phase. The NbO–Fe_2O_3 system was the only one in which Fe^{2+} ions were detected by Mössbauer measurements. The favorable substitution of Fe^{2+} for Nb^{2+} in the octahedral sites in the NbO lattice was observed after 12 h milling for $x=0.7$. At $x=0.5$ both Nb^{2+}-doped hematite and Fe^{3+}-doped NbO were obtained. In the NbO_2–Fe_2O_3 and Nb_2O_5–Fe_2O_3 systems a formation of orthorhombic $FeNbO_4$ compound was observed, in which Fe^{3+} cations were detected. For the highest concentration of NbO_2 ($x=0.7$) iron was completely incorporated into the $FeNbO_4$ phase after 12 h milling. In the case of the Nb_2O_5–Fe_2O_3 system the molar concentration played a major role in the synthesis of the ternary compound. The concentrations of $x=0.3$ and 0.5 were the most favorable for the formation of $FeNbO_4$. Furthermore, the formation of Nb-doped hematite was significantly suppressed by the constitution of non-magnetic iron niobate for $x \geq 0.3$. The estimated values of average grain sizes of the phases detected by XRD decreased gradually with the increase of milling time and in most cases they were below 20 nm after 12 h milling. It was found that ball milling had a strong influence on the thermal behavior of the powders as compared with the starting mixtures. The weight loss values observed up to about 600 °C were rather small and did not exceed 2.5% for all studied samples. They were assigned mainly to a partial decomposition of hematite to magnetite.

Acknowledgment

This work was supported by the National Science Foundation.

Appendix A. Supporting information

Supplementary data associated with this article can be found in the online version at http://dx.doi.org/10.1016/j.ceramint.2012.12.040.

References

[1] J. Ge, T. Huynh, Y. Hu, Y. Yin, Hierarchical magnetite/silica nanoassemblies as magnetically recoverable catalyst-supports, Nano Letters 8 (2008) 931–934.

[2] A.C. Silva, D.Q.L. Oliveira, L.C.A. Oliveira, A.S. Anastacio, T.C. Ramalho, J.H. Lopes, Nb-containing hematites $Fe_{2-x}Nb_xO_3$: the role of Nb^{5+} on the reactivity in presence of the H_2O_2 or ultraviolet light, Applied Catalysis A 357 (2009) 79–84.

[3] S. Krishnamoorthy, J.A. Rivas, M.D. Amiridis, Catalytic oxidation of 1,2-dichlorobenzene over supported transition metal oxides, Journal of Catalysis 193 (2000) 264–272.

[4] M. Sorescu, L. Diamandescu, A. Tomescu, D. Tarabasanu-Mihaila, V. Teodorescu, Structure and sensing properties of $0.1SnO_2$–0.9α-Fe_2O_3 system, Materials Chemistry and Physics 107 (2008) 127–131.

[5] M.S. Ramos, M.S. Santos, L.P. Gomes, A. Albornoz, M.C. Rangel, The influence of dopants on the catalytic activity of hematite in the ethylbenzene dehydrogenation, Applied Catalysis A 341 (2008) 12–17.

[6] R. Sani, A. Beitollahi, Phase evolution and magnetic properties of Co/α-Fe_2O_3 powder mixtures with different molar ratios treated by mechanical alloying, Journal of Non-Crystalline Solids 354 (2008) 4635–4643.

[7] M.I. Ivanovskaya, D.A. Kotsikau, A. Taurino, P. Siciliano, Structural distinctions of $Fe_2O_3-In_2O_3$ composites obtained by various sol–gel procedures and their gas-sensing features, Sensors and Actuators B 124 (2007) 133–142.

[8] Y. Yu, C. Feng, C. Li, Y. Yang, W. Yao, H. Yan, Formation of columbite-type precursors in the mixture of MgO–Fe_2O_3–Nb_2O_5 and the effects on fabrication of perovskites, Materials Letters 51 (2001) 490–499.

[9] E. Traversa, S. Matsushima, G. Okada, Y. Sadaoka, Y. Sakai, K. Watanabe, NO_2 sensitive $LaFeO_3$ thin films prepared by r.f. sputtering, Sensors and Actuators B 25 (1995) 661–664.

[10] H. Meixner, U. Lampe, Metal oxide sensors, Sensors and Actuators B 33 (1996) 198–202.

[11] N. Yamazoe, Y. Teraoka, Oxidation catalysis of perovskites—relationships to bulk structure and composition (valency, defect, etc.), Catalysis Today 8 (1990) 175–199.

[12] L.C.A. Oliveira, F. Zaera, I. Lee, D.Q. Lima, T.C. Ramalho, A.C. Silva, E.M.B. Fonseca, Nb-doped hematites for decomposition of isopropanol: evidence of surface reactivity by in situ CO adsorption, Applied Catalysis A 368 (2009) 17–21.

[13] C. Sanchez, M. Hendewerk, K.D. Sieber, G.A. Somorjai, Synthesis, bulk, and surface characterization of niobium-doped Fe_2O_3 single crystals, Journal of Solid State Chemistry 61 (1986) 47–55.

[14] H. Miyake, H. Kozuka, Photoelectrochemical properties of Fe_2O_3–Nb_2O_5 films prepared by sol–gel method, The Journal of Physical Chemistry B 109 (2005) 17951–17956.

[15] L.C.A. Oliveira, M. Gonçalves, M.C. Guerreiro, T.C. Ramalho, J.D. Fabris, M.C. Pereira, K. Sapag, A new catalyst material based on niobia/iron oxide composite on the oxidation of organic contaminants in water via heterogeneous Fenton mechanisms, Applied Catalysis A 316 (2007) 117–124.

[16] L.C.A. Oliveira, T.C. Ramalho, E.F. Souza, M. Gonçalves, D.Q.L. Oliveira, M.C. Pereira, J.D. Fabris, Catalytic properties of goethite prepared in the presence of Nb on oxidation reactions in water: computational and experimental studies, Applied Catalysis B 83 (2008) 169–176.

[17] M.A. Tena, G. Garcia-Belmonte, J. Bisquert, P. Escribano, M.T. Colomer, J.R. Jurado, Impedance spectroscopy studies of orthorhombic $FeNbO_4$, Journal of Materials Science 31 (1996) 2043–2046.

[18] E. Schmidbauer, J. Schneider, Electrical resistivity, thermopower, and ^{57}Fe Mössbauer study of $FeNbO_4$, Journal of Solid State Chemistry 134 (1997) 253–264.

[19] W.T.A. Harrison, A.K. Cheetham, Structural and magnetic properties of $FeNbO_4$-II, Materials Research Bulletin 24 (1989) 523–527.

[20] H. Ehrenberg, G. Wltschek, R. Theissmann, H. Weitzel, H. Fuess, F. Trouw, The magnetic structure of $FeNbO_4$, Journal of Magnetism and Magnetic Materials 218 (2000) 261–265.

[21] K.I. Gnanasekar, V. Jayaraman, E. Prabhu, T. Gnanasekaran, G. Periaswami, Electrical and sensor properties of $FeNbO_4$: a new sensor material, Sensors and Actuators B 55 (1999) 170–174.

[22] R.S. Roth, J.L. Waring, Ixiolite and other polymorphic types of $FeNbO_4$, American Mineralogist 49 (1964) 242–246.

[23] S. Ananta, R. Brydson, N.W. Thomas, Synthesis, formation and characterisation of $FeNbO_4$ powders, Journal of European Ceramic Society 19 (1999) 489–496.
[24] G.H. Chen, Iron niobate derived from mechanochemically activated oxides, Journal of Alloys and Compounds 381 (2004) 309–312.
[25] M. Sorescu, T.H. Xu, L. Diamandescu, Mechanochemical synthesis and characterization of $x In_2O_3 \cdot (1-x)\alpha$-$Fe_2O_3$ nanostructure system, Journal of Materials Science 46 (2011) 2350–2358.
[26] M. Sorescu, T.H. Xu, L. Diamandescu, D. Hileman, Synthesis and characterization of indium oxide-hematite magnetic ceramic solid solution, Hyperfine Interactions 199 (2011) 365–386.
[27] M. Sorescu, T.H. Xu, J.D. Burnett, J.A. Aitken, Investigation of $LaFeO_3$ perovskite growth mechanism through mechanical ball milling of lanthanum and iron oxides, Journal of Materials Science 46 (2011) 6709–6717.
[28] M. Sorescu, T.H. Xu, L. Diamandescu, Synthesis and characterization of $x TiO_2 \cdot (1-x)\alpha$-$Fe_2O_3$ magnetic ceramic nanostructure system, Materials Characterization 61 (2010) 1103–1118.
[29] M. Sorescu, L. Diamandescu, A. Tomescu, S. Krupa, Synthesis and sensing properties of zirconium-doped hematite nanoparticles, Physica B 404 (2009) 2159–2165.
[30] M. Sorescu, L. Diamandescu, V.S. Teodorescu, Structure and characterization of cerium-doped hematite nanoparticles, Physica B 403 (2008) 3838–3845.
[31] D. Malczewski, A. Grabias, ^{57}Fe Mössbauer spectroscopy and X-ray diffraction study of complex metamict minerals, Part II. Hyperfine Interactions 186 (2008) 75–81.
[32] M. Sorescu, T.H. Xu, Particle size effects on the thermal behavior of hematite, Journal of Thermal Analysis and Calorimetry 107 (2012) 463–469.